Chemical Engineering Science 318 (2025) 122185

Contents lists available at ScienceDirect

Chemical Engineering Science

journal homepage: www.elsevier.com/locate/ces

The effect of particle surface roughness and biofilm accumulation on the pressure drop over a biofilter

R. J. Van Velden [a], S. Woudberg [a,*], E. Dumont [b], H. Fidder [c,d], J.Th.M. De Hosson [c]

[a] Department of Mathematical Sciences, Applied Mathematics Division, Stellenbosch University, Private Bag X1, 7602, Matieland, South Africa
[b] UMR 6144, Nantes Université, IMT Atlantique, CNRS, GEPEA, F-44000, Nantes, France
[c] Department of Applied Physics, Zernike Institute for Advanced Materials, University of Groningen, 9747 AG, Groningen, The Netherlands
[d] Department of Mechanical Engineering, Cape Peninsula University of Technology, Cape Town, South Africa

ARTICLE INFO

Keywords:
Granular
Porous media
Analytical modelling
Microstructure
Biofiltration
Surface roughness
Sphericity

ABSTRACT

In this study, the pressure drop prediction of the existing granular rectangular Representative Unit Cell (RUC) model, which already accounts for biofilm development and sphericity, is adapted to include particle surface roughness. The novelty of this study is that a surface roughness factor is derived based on physical principles. It was found to be a function of the average height and number of roughness elements, the porosity as well as the particle diameter. This factor is included in both the Darcy and inertial Reynolds number flow terms. The proposed model includes no empirical coefficients and is validated against experimental data for a biofilter, operated over 107 days, with expanded schist as packing material. It was found that a decrease in average particle shape factor produced an increase in surface roughness over time. The average shape factor was also introduced in order to increase the interstitial form drag coefficient. The average surface roughness of the packing material was measured with a confocal microscope, by utilizing white light microscopy, and the value was used in the pressure gradient prediction of the RUC model. The proposed model is compared to a modified Ergun equation, adjusted to be applicable to biofilters, and satisfactory results are obtained. A sensitivity analysis is also performed on the average height of surface roughness elements, particle diameter, and average particle shape factor. The proposed model is an improvement on the existing models from the literature considered in this study.

1. Introduction

Biofilters have become an increasingly popular topic in the field of porous media. A biofilter is a device created for the purpose of controlling hazardous substances, such as hydrogen sulfide (H_2S), in an ecologically friendly manner (Yang and Allen, 1994). Biofilters are widely applicable in the industry and can also be used for adsorption of air contaminants produced by factories and other industrial processes (Morgan-Sagastume et al., 2001), the treatment of rendering odours produced by waste facilities (Prokop and Bohn, 1985), and the controlling of volatile organic compounds (VOC's) emitted from various sources (Alonso et al., 1997).

A biofilter consists of a porous bed, consisting of a packing material and a layer of moisture, known as biofilm. Biofilm is made up of microorganisms that can degrade pollutant substances from a contaminated air stream pumped through the packing material (Devinny et al., 2017; Soreanu and Dumont, 2020). In addition to the packing material and inclusion of the biofilm, efficient and adequate removal capabilities in biofiltration are also dependent on optimal experimental operation conditions. Biofilters can furthermore be classified by their structure (e.g. open or closed beds), packing material (e.g. inert or organic materials), and their applications (e.g. water or air purification).

Predicting the pressure drop over a biofilter used for H_2S removal is essential for: Operational efficiency; cost control; design accuracy; performance reliability; maintenance planning and health and environmental safety. This makes it a key parameter in the engineering and management of biofiltration systems (e.g. Chen et al., 2019). For research and industrial scale-up, being able to predict the pressure drop supports accurate modelling of mass transfer, kinetics, and airflow dynamics. There are thus numerous factors that may influence biofilter performances for gas treatment, including gas concentration, EBRT (Empty Bed Residence Time), moisture, pH, temperature and pressure drops (Dumont, 2017). These factors allow for either kinetically controlled or mass transfer biofilter efficiency. The former refers to how fast microorganisms degrade pollutants reaching the biofilm, whereas the latter refers to how well pollutants move from the gas phase into the

* Corresponding author.
E-mail addresses: rocco@sun.ac.za (R. J. Van Velden), fidder@sun.ac.za (S. Woudberg), eric.dumont@imt-atlantique.fr (E. Dumont), h.fidder@rug.nl (H. Fidder), j.t.m.de.hosson@rug.nl (J.Th.M. De Hosson).

https://doi.org/10.1016/j.ces.2025.122185
Received 1 May 2025; Received in revised form 29 May 2025; Accepted 5 July 2025
Available online 11 July 2025

Nomenclature

Notation	Description
A, B	viscous and inertial constants in modified Ergun equation []
$A_{p_{\|\|}}$	streamwise cross-sectional flow area in RUC [m^2]
c_d	interstitial form drag coefficient [ ]
d	RUC cell size [m]
d_s	average particle diameter [m]
Δp	streamwise pressure drop [Pa]
h_{avg}	average height of roughness elements [m]
k	amount of roughness elements []
L	packed bed length [m]
L_f	biofilm thickness [m]
n	coordination number [ ]
q	superficial velocity [m·s^{-1}]
R	radius of spherical particle [m]
R_a	arithmetic average roughness value [m]
R_q	root mean squared average roughness value [m]
$\mathcal{R}$	particle surface roughness variable coefficient [ ]
$S_{\|\|}$	total streamwise surface areas in RUC [m^2]
$S_{\perp}$	total transverse surface areas in RUC [m^2]
S_{face}	cross-sectional area of solid “facing” upstream [m^2]
S_s	total surface area of RUC solid [m^2]
U_f	total fluid volume in RUC [m^3]
U_s	total solid volume in RUC [m^3]
U_o	total (fluid and solid) volume in RUC [m^3]
$w_{\|\|}$	streamwise average channel velocity [m · s^{-1}]
α	particle surface roughness constant coefficient [ ]
β	average channel velocity ratio [ ]
δ	parameter in numerator of roughness factor $\mathcal{R}$ [ ]
ϵ	porosity [ ]
ϵ_f	biofilm affected porosity [ ]
ϵ_o	initial biofilter porosity (i.e. with no biofilm) [ ]
μ	fluid viscosity [kg · m^{-1} · s^{-1}]
ξ	geometric coefficient [ ]
ρ	fluid density [kg · m^{-3}]
σ	parameter in denominator of roughness factor $\mathcal{R}$ [ ]
$\tau_{w_{\|\|}}$	magnitude of average wall shear stress on streamwise surfaces [N · m^{-2}]
$\tau_{w_{\perp}}$	magnitude of average wall shear stress on transverse surfaces [N · m^{-2}]
ϕ	particle sphericity / average particle shape factor [ ]
ψ	geometric factor [ ]

Superscripts

Notation:	Description:
$*$	pertains to roughness [ ]

biofilm where biodegradation occurs. Dumont (2017) mentions that a change in EBRT has a notable influence on the limiting step, which refers to the slowest process that influences the overall biofilter efficiency, while a change in temperature affects biological reactions and mass transfer in opposite ways. Furthermore, a short measurement time for pressure drops (i.e. lower than 1–2 hours) implies that a steady-state assumption is realistic. This yields a stable biofilter performance and efficiency over time, meaning that variables such as concentration and mass transfer rates are assumed to be constant over the measurement period.

This main focus of this study is on providing a novel analytical equation for the pressure drop prediction, with the originality being the inclusion of the effect of particle surface roughness. It relates to previous studies on overall biofilter operation and optimization conducted by Dumont et al. (2016) and Dumont et al. (2012).

Dumont et al. (2016) conducted an empirical study on experimental biofiltration data from Dumont et al. (2012) for a closed bed biofilter, with an inert packing material, namely expanded schist, for H_2S degradation (e.g. air purification). Three granular porous media models were investigated and compared using Excel solver to predict the porosity change and biofilm thickness over time.

The first model investigated by Dumont et al. (2016) is the notable modified Ergun equation, proposed by Morgan-Sagastume et al. (2001), i.e.

$$\frac{\Delta p}{L} = \frac{A\,(1-\epsilon)^2}{\epsilon^{3.6}\,\phi^2\,d_s^2}\,\mu\,q + \frac{B\,(1-\epsilon)}{\epsilon^{3.6}\,\phi\,d_s}\,\rho\,q^2, \tag{1}$$

where Δp is the streamwise pressure drop over a packed bed length of L, q is the magnitude of the superficial velocity, ϵ is the porosity, μ the fluid viscosity, ρ the fluid density, ϕ the sphericity and d_s the particle diameter. The coefficients $A = 180$ and B are empirical, where the latter is said to vary with particle surface roughness. Surface roughness refers to the microscopic irregularities on the surfaces of particles and is usually introduced as a constant (mostly empirically based) that lacks physical meaning. Due to the complexity and size of the irregularities, it has remained a challenging task to quantify its contribution to the pressure gradient.

The capillary-tube model, forming the basis of the Ergun equation, has also been used extensively in the field of fractal analysis to provide permeability models involving analytical fractal parameters instead of empirical curve-fitting parameters. In the fractal models the pore (or grain) size distribution and tortuosity are defined by fractal dimensions in order to describe the inherent complex and irregular nature of the pore space. The first permeability model was provided by Yu and Cheng (2002), followed by a notable improvement by Xu and Yu (2008). The latter two studies form the foundational framework of the majority of fractal models that followed in the years thereafter. Hu et al. (2020), for instance, adapted the fractal permeability models of Yu and Cheng (2002) in combination to that of Xu and Yu (2008) by providing an alternative expression for the total length of the porous medium together with a maximum pore diameter for both a loose and compact cluster of particles. In order to account for particle surface roughness of granular porous media, Yang et al. (2015) introduced the relative roughness, proposed by Yang et al. (2014) for rectangular microchannels, into the capillary-tube model. Wu and Yu (2007),Huang et al. (2020) and Xu et al. (2024) have presented fractal models for predicting the pressure drop over granular porous media, applicable to both the Darcy and Forchheimer flow regimes, but excluding the effect of particle surface roughness. Xiao et al. (2023), furthermore, adapted the fractal permeability model of Xu and Yu (2008) by incorporating the effect of converging and diverging capillaries as well as the fractal roughness parameter proposed by Yang et al. (2014). Fractal models have also been developed for other types of porous structures. Xiao et al. (2021) have, for example, presented a fractal model for fibrous media by considering flow through a single tortuous capillary of which the surfaces are rough. Tu et al. (2024), furthermore, provided a fractal permeability model for tree-like branched networks consisting of non-uniform capillary diameters. The drawback of the fractal models is, however, that it is often extremely difficult to assign values to the fractal parameters in compliance with the physical measurable parameters.

Another model investigated by Dumont et al. (2016) is the pressure gradient model developed by Comiti and Renaud (1989) for parallelepipedal particles.

The third model investigated is the granular rectangular Representative Unit Cell (RUC) model, developed over the years by, amongst others, Du Plessis and Masliyah (1991), Du Plessis (1994) and Du Plessis and Woudberg (2008). The model was developed to serve as an analytical derivation of the empirical Ergun equation. The pressure gradient predicted by the RUC model is given by

$$\frac{\Delta p}{L} = \frac{25.4\,(1-\epsilon)^{4/3}}{\phi^2\, d_s^2 \left(1-(1-\epsilon)^{1/3}\right)\left(1-(1-\epsilon)^{2/3}\right)^2}\,\mu\, q + \frac{\alpha\, c_d\,(1-\epsilon)}{2\,\phi\, d_s\,\epsilon\left(1-(1-\epsilon)^{2/3}\right)^2}\,\rho\, q^2, \tag{2}$$

where $c_d = 1.9$ is an interstitial form drag coefficient and α is a particle roughness coefficient of which the value is assigned to be in accordance with the coefficient B in the modified Ergun equation (i.e. Eq. (1)). The objective of this study is to assign physical significance to this parameter in order to be consistent with the analytical modelling procedure in the derivation of the RUC model.

In the study of Dumont et al. (2016), the value for B was treated as a tuning factor for the modified Ergun model (ranging from 1.62 to 4.95) and corresponds to the product of $\alpha\, c_d$ for the RUC model, which was kept constant over time. Dumont et al. (2016) mentioned that it would be beneficial to have the latter product vary over time for better prediction of the porosity, since surface roughness is a dominating factor in biofilm-development according to Van Loosdrecht et al. (1995). This served as another motivation to investigate the quantification of the surface roughness parameter based on physical reasoning.

A follow-up study was done by Woudberg et al. (2019) to adapt the existing granular RUC model (i.e. Eq. (2)) to take biofilm development into account. This was done by adapting the biofilm-affected porosity ϵ_f and biofilm thickness L_f relationship proposed by Alonso et al. (1997),

$$\epsilon_f = 1-(1-\epsilon_0)\left[\left(1+\frac{L_f}{\phi R}\right)^3 - \frac{n}{4}\left(\frac{L_f}{\phi R}\right)^2\left(2\frac{L_f}{\phi R}+3\right)\right], \tag{3}$$

by introducing the sphericity, where R is the radius of a spherical particle, ϵ_0 is the initial bed porosity and n is the coordination number.

Dumont et al. (2016) calculated the sphericity using Excel solver with the modified Ergun equation, together with experimental data on the first day when no biofilm was yet present. They calculated the sphericity to be $\phi = 0.85$ and kept this value constant over time, whilst changing the tuning factor B in order to account for surface roughness. This implies that the biofilm development did not change the shape of the schist particle over time. Dumont et al. (2016) do, however, mention that if a larger variation in porosity due to biofilm development is observed over time, then a variable sphericity should be considered.

Woudberg et al. (2019) kept the roughness constant and varied the sphericity over time. They quantified the sphericity for a cluster of particles in contact with each other and with biofilm overlap in terms of the biofilm thickness and coordination number and mentioned that the effect of the sphericity on the biofilm-affected porosity and pressure drop predictions is considerable.

The modelling integration of the pressure drop equations and biofilm-affected porosity is achieved by replacing the porosity in Eqs. (1) and (2) with the biofilm-affected porosity, as given by Eq. (3). Eqs. (1) and (2) then become

$$\frac{\Delta p}{L} = \frac{A\,(1-\epsilon_f)^2}{\epsilon_f^{3.6}\, d_s^2}\,\mu\, q + \frac{B\,(1-\epsilon_f)}{\epsilon_f^{3.6}\, d_s}\,\rho\, q^2, \tag{4}$$

and

$$\frac{\Delta p}{L} = \frac{25.4\,(1-\epsilon_f)^{4/3}}{\phi^2\, d_s^2 \left(1-(1-\epsilon_f)^{1/3}\right)\left(1-(1-\epsilon_f)^{2/3}\right)^2}\,\mu\, q + \frac{\alpha\, c_d\,(1-\epsilon_f)}{2\,\phi\, d_s\,\epsilon_f\left(1-(1-\epsilon_f)^{2/3}\right)^2}\,\rho\, q^2, \tag{5}$$

respectively, with $c_d = 1.9$ and $\alpha = 2$.

As noted earlier, Woudberg et al. (2019) varied the sphericity, whilst keeping the roughness constant. Note that the sphericity is not included in Eq. (4). They worked with an upper and lower bound for ϕ (i.e. $0.5 \le \phi \le 1$) for the granular RUC model, however, kept the value of ϕ constant for the modified Ergun equation. They noticed that the modified Ergun equation did not predict the data accurately in the later stages of biofilter operation and contributed this to the lack of a variable sphericity and surface roughness. Furthermore, they concluded that the average range of sphericity for which the RUC gives the most accurate predictions is $0.6 \le \phi \le 0.8$, which is less that the suggested sphericity of $\phi = 0.85$ used by Dumont et al. (2016). No explanation as to why certain sphericity values work better than others was offered. Woudberg et al. (2019) suggested that the influence of surface roughness in combination with the sphericity is worthwhile to investigate.

This study serves as an extension and present novel approaches to the work done by Dumont et al. (2016) and Woudberg et al. (2019) by (i) providing physical meaning to the empirical roughness parameter used by Dumont et al. (2016) as a fitting parameter and also to the constant particle roughness coefficient introduced by Woudberg et al. (2019) into the RUC model and (ii) providing a first-order approach for introducing the interdependence of sphericity (or shape factor) on the surface roughness, which was kept constant by Dumont et al. (2016), but varied independently to a constant particle roughness by Woudberg et al. (2019). This will be done by deriving a roughness factor from physical principles as a function of the average roughness height, number of roughness elements, average particle shape factor, average particle diameter and porosity. This step in the analytical modelling procedure adds originality to this study.

Section 2 presents the adapted analytical RUC modelling procedure as well as the adapted model geometry to include the effects of surface roughness on the pressure drop. Section 3 gives an outline of the experimental procedure followed in order to measure and quantify the particle surface roughness. The model validation is presented in Section 4, based on the experimental data sets of Allen et al. (2013) involving airflow through rough wooden cubes and Dumont et al. (2012) for H_2S biofiltration. Finally a sensitivity analysis is provided in Section 5 to investigate the influence of key parameters on the model predictions.

2. Adapted RUC model

Surface roughness is difficult to characterize and model with precision. Gadelmawla et al. (2002) provide mathematical definitions of about 59 roughness parameters and divide them into three categories, namely, amplitude, spacing and hybrid parameters. Amongst the amplitude parameters, the arithmetic average height (R_a) and root mean square or rms (R_q) roughness are the most commonly used and defined parameters.

Most rough surfaces in modern days are classified as “self-affine” or “self-similar”, with the former being the general concept. Self-affinity refers to fractal structures that scale differently in different directions, whereas self-similar structures scale uniformly in all directions. Self-affine structures are very complex and are generally characterized by at least two parameters, namely a rms roughness amplitude and lateral correlation length (Palasantzas and De Hosson, 2000).

In practice it can be difficult to obtain all these roughness parameters from sample measurements and in analytical modelling it is often difficult to incorporate them. For self-affine surfaces often the “degree of roughness” is introduced through a roughness exponent and this is even more difficult to quantify analytically.

This study incorporates a simple geometric adaptation to characterize and model roughness by using the amplitude parameter R_a, defined as the average height of roughness elements h_{avg}, as the only roughness parameter.

The geometric adaptation comprises of representing the surface roughness as microscopic cubes (or roughness elements) added onto the

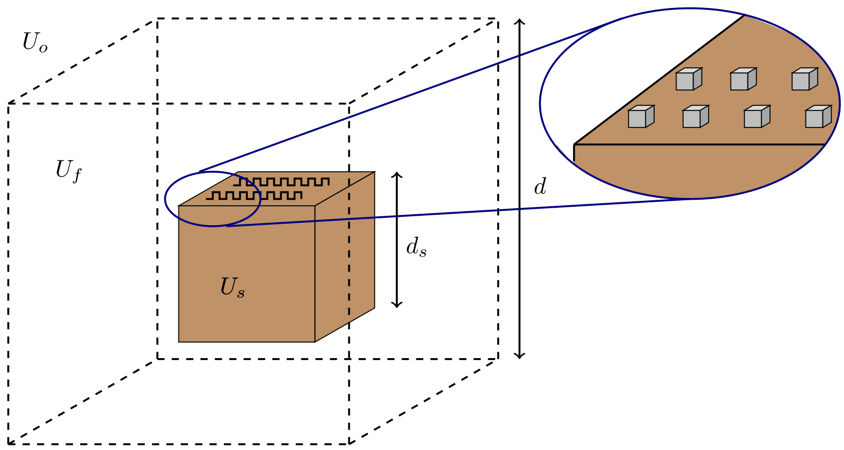

Fig. 1. Granular RUC model including surface roughness.

surface of the existing granular RUC solid, as schematically illustrated in Fig. 1.

In Fig. 1, U_o denotes the total (fluid and solid volume in the RUC, U_f is the total fluid volume and U_s the total solid volume. The cell size of the RUC is represented by d.) Although the roughness elements are indicated only on the top surface of the solid in Fig. 1, the following assumptions is made:

Assumption 2.1. *The roughness elements cover all six faces of the solid cube in the RUC model.*

Assumption 2.2. *The distribution of roughness elements on the total outer solid surface will not be accounted for, only the total number of elements (as an order of magnitude estimate).*

Assumption 2.2 implies that self-affinity is excluded and thus implies that the lateral correlation length between roughness elements need not be accounted for in calculations, as well as an exponent for the "degree of roughness".

It is important to note that the solid cube in the RUC model represents the average solid geometry of the real granular porous medium. For the sake of completeness, the derivation of the pressure gradient prediction of the existing granular RUC model (Du Plessis and Woudberg, 2008) is given in Appendix A. The proposed adapted geometric RUC model is based on the following assumption:

Assumption 2.3. *The added roughness elements contribute to the total outer surface area of the solids (particles) and do not contribute to the total volume of the solids.*

The justification of this assumption is in noting that the microscopic elements are sufficiently small (i.e. micrometers) in comparison to the granular solids (i.e. millimeters), so that their contribution to the total volume of the solids is negligible. However, the surface area of the elements in comparison to the total surface area of the solids is not insignificant and this contribution will be taken into account.

In comparison to the existing (smooth) granular RUC model, Assumption (2.3) implies that (i) the definition of the porosity ϵ does not change, (ii) the particle diameter d_s does not change, and (iii) the RUC dimension d does not change (see Fig. 1). All the geometric RUC parameters that change as a result of the roughness will be indicated with a "*" as opposed to the smooth/non-affected parameters indicated without a "*", i.e. representing the same notation used for the existing model. The surface roughness will be incorporated into the total streamwise surface area $S^*_{||}$, the total transverse surface area $S^*_{\perp}$, the total cross-sectional area of the solids "facing" upstream S^*_{face}, and the geometric factor ψ^*. The average streamwise wall shear stress $\tau_{w_{||}}$ (Eq. (A.5)) is also affected by the added roughness, but specifically through the average streamwise pore velocity $w_{||}$ which, in turn, is defined in terms of ψ. The roughness is therefore explicitly incorporated into ψ and implicitly into $\tau_{w_{||}}$. The "smooth" parameters of the model of Du Plessis and Woudberg (2008) are defined in Appendix A, which provides a short summary of this model. Adapting Eqs. (A.7) and (A.9) in Appendix A for the Darcy and Forchheimer regimes, respectively, yields

$$\frac{\Delta p}{L} = \frac{6(S^*_{||} + \beta\,\xi\,S^*_{\perp})}{(d-d_s)\,d^3}\,\frac{\psi^{*2}}{\epsilon^2}\,\mu\,q, \tag{6}$$

and

$$\frac{\Delta p}{L} = \frac{S^*_{face}\,\psi^{*2}}{2\,\epsilon^3\,U_o}\,c_d\,\rho\,q^2. \tag{7}$$

Note that the pore width $d - d_s$, as well as the total RUC volume U_o, the RUC solid volume U_s, and the RUC fluid volume U_f indicated in Fig. 1, remain unchanged due to Assumption 2.3. The coefficient β was introduced by Du Plessis and Woudberg (2008) to account for the difference in the average streamwise and transverse channel velocities in the RUC model and the geometric coefficient ξ for the reduction in tortuosity as a result of the splitting of the streamtube in the transverse channels of a staggered array.

Since the model does not account for the distribution of roughness elements on each face of the RUC solid, but rather the quantification thereof in terms of added surface roughness, Assumption 2.4 is made:

Assumption 2.4. *There are k identical roughness elements on each face of the granular RUC model, where k is merely an order of magnitude estimate, represented as a positive integer.*

Let each cubic roughness element have a dimension of h_{avg}, representing the average measured height of the real rough packing material. As a result of Assumption 2.1, there is a total of $6\,k$ roughness elements on the RUC solid. A value of $k = 0$ represents a smooth surface with no roughness elements. The procedure of determining an upper and lower bound for k will be outlined in Section 4 for different experimental data sets.

The 2D cross-sectional area of the RUC solid is a square with $\sqrt{k}$ roughness elements on each side. There is a total of $4\sqrt{k}$ roughness elements on the solid perimeter. Recall that it is assumed that d_s remains unchanged, irrespective of the additional h_{avg} introduced through the roughness elements.

A single face of the existing granular RUC solid has a surface area of d_s^2. If an arbitrary face of the solid is viewed in a perpendicular manner after the addition of roughness elements, the face will look identical to that of a smooth face, however, additional surface area emerges from the four side faces of each individual roughness element. The total additional surface area that results from roughness elements per face of the rough RUC solid are thus $4\,k\,h^2_{avg}$ and the total additional volume of roughness elements per face of the rough RUC solid is hence $k\,h^3_{avg}$.

As mentioned, this volume is assumed to be negligible compared to the total volume of the RUC solid.

After the additional surface area of the roughness elements is added to each face of the solid, the total streamwise surface area becomes $S^*_{||} = 4\,(d_s^2 + 4\,k\,h_{avg}^2)$. It hence follows that

$$S^*_{||} = S_{||}\left(1 + \frac{4\,k\,h_{avg}^2}{d_s^2}\right) = S_{||}\,(1+\delta), \tag{8}$$

where

$$\delta = \frac{4\,k\,h_{avg}^2}{d_s^2}. \tag{9}$$

Including the sphericity into Eq. (9), yields

$$\delta = \frac{4\,k\,h_{avg}^2}{(\phi\,d_s)^2}. \tag{10}$$

It results in a similar manner that the total transverse surface area becomes $S^*_{\perp} = 2\,(d_s^2 + 4\,k\,h_{avg}^2)$. After factorization and simplification, it follows that

$$S^*_{\perp} = S_{\perp}\left(1 + \frac{4\,k\,h_{avg}^2}{d_s^2}\right) = S_{\perp}\,(1+\delta), \tag{11}$$

where the expression for δ is given by Eq. (9).

Incorporating the extra surface area to S_{face} as a result of surface roughness, yields $S^*_{face} = d_s^2 + 4\,k\,h_{avg}^2$. After simplification it follows that

$$S^*_{face} = S_{face}\left(1 + \frac{4\,k\,h_{avg}^2}{d_s^2}\right) = S_{face}\,(1+\delta). \tag{12}$$

Accounting for the additional surface area of the roughness elements, the streamwise cross-sectional area becomes $A^*_{p_{||}} = d^2 - d_s^2 - 4\,\sqrt{k}\,h_{avg}^2$. Expressing ψ^* in terms of $A^*_{p_{||}}$ yields (see Appendix A)

$$\psi^* = \frac{U_f}{A^*_{p_{||}}\,d} = \frac{d^3 - d_s^3}{(d^2 - d_s^2 - 4\,\sqrt{k}\,h_{avg}^2)\,d} = \frac{\epsilon}{1 - (1-\epsilon)^{2/3} - \frac{4\,\sqrt{k}\,h_{avg}^2}{d^2}}, \tag{13}$$

from which it follows that

$$\psi^* = \psi\,\frac{1}{1 - \frac{4\,\sqrt{k}\,h_{avg}^2}{d_s^2\left[(1-\epsilon)^{-2/3} - 1\right]}} = \psi\,\frac{1}{1-\sigma}, \tag{14}$$

where

$$\sigma = \frac{4\,\sqrt{k}\,h_{avg}^2}{d_s^2\left[(1-\epsilon)^{-2/3} - 1\right]}. \tag{15}$$

For the adapted RUC model of the present study, ϕ will be called the "average particle shape factor", instead of the "sphericity". For a bed of uniform particle shapes, the term sphericity, which is indeed also a shape factor, can be used in the proposed RUC model prediction. However, for a bed of nonuniform particle shapes, the sphericity rather represents an average shape factor, with some properties similar to that of the sphericity, but others not, as will be outlined in the remainder of this study. The *average* property also complies with all the other RUC model input parameters, since the whole concept of the RUC model is to represent the *average* pore-scale geometry. The average shape factor should therefore not be regarded as an exact value related to a specific particle shape. For beds of uniformly shaped particles it does, but not generally for nonuniform shapes. Including the average particle shape factor into Eq. (15), yields

$$\sigma = \frac{4\,\sqrt{k}\,h_{avg}^2}{(\phi d_s)^2\left[(1-\epsilon)^{-2/3} - 1\right]}. \tag{16}$$

Note that the average shape factor was introduced in the same way as the sphericity into the predictive equations, i.e. by multiplyingthe particle diameter by this factor. In the next subsection the pressure gradient predicted by the granular RUC model with roughness included will be obtained for the Darcy and Forchheimer flow regimes.

2.1. Darcy flow regime

Substituting Eqs. (8), (11) and (14) into Eq. (6) after which the average particle shape factor is incorporated, leads to

$$\frac{\Delta p}{L} = \frac{6(S_{||} + \beta\,\xi\,S_{\perp})}{(d - d_s)\,d^3}\,\frac{\psi^2}{\epsilon^2}\left[\frac{1+\delta}{(1-\sigma)^2}\right]\mu\,q. \tag{17}$$

Following the same analytical modelling procedure as with the derivation of the existing model and incorporating the expressions for $\psi, S_{||}, S_{\perp}, d_s, \beta$ and ξ, the resulting pressure gradient for the Darcy flow regime, including roughness and average particle shape factor, can be written as

$$\frac{\Delta p}{L} = \frac{25.4\,(1-\epsilon)^{4/3}}{(\phi\,d_s)^2\left(1 - (1-\epsilon)^{1/3}\right)\left(1 - (1-\epsilon)^{2/3}\right)^2}\,\mathcal{R}\,\mu\,q, \tag{18}$$

where

$$\mathcal{R} = \frac{1+\delta}{(1-\sigma)^2} = \frac{1 + \left(4\,k\,h_{avg}^2\right)\Big/\left(\phi\,d_s\right)^2}{\left[1 - \left(4\,\sqrt{k}\,h_{avg}^2\right)\Big/\left([\phi d_s]^2[(1-\epsilon)^{-2/3} - 1]\right)\right]^2} \tag{19}$$

is the roughness factor, which is a function of the average roughness height, number of roughness elements, average particle shape factor, average particle diameter and porosity.

2.2. Forchheimer flow regime

Substituting Eqs. (12) and (14) into Eq. (7), yields

$$\frac{\Delta p}{L} = \frac{S_{face}\,\psi^2}{2\,\epsilon^3\,U_o}\left[\frac{1+\delta}{(1-\sigma)^2}\right]c_d\,\rho\,q^2. \tag{20}$$

Incorporating the expressions for S_{face}, U_o, ψ and d_s, the resulting pressure gradient for the Forchheimer regime including roughness and average particle shape factor, leads to

$$\frac{\Delta p}{L} = \frac{c_d\,(1-\epsilon)}{2\left(1 - (1-\epsilon)^{2/3}\right)^2\epsilon\,\phi^{3/2}\,d_s}\,\mathcal{R}\,\rho\,q^2, \tag{21}$$

where $\mathcal{R}$ is also given by Eq. (19). Note that the average particle shape factor in Eq. (21) has a different power to that of Eq. (5), which has a linear power in ϕ. The reason is due to the interstitial form drag coefficient c_d also being adapted in this study to include the average particle shape factor, since the form drag coefficient is generally shape-dependent. The previous constant c_d is replaced by $c_d/\phi^{1/2}$, hence producing $\phi^{3/2}$ in Eq. (21).

Fig. 2 shows $c_d = c_d\phi^{\nu}$ versus ϕ for $\nu = -1$ and $\nu = -0.5$, respectively, together with a starting value of $c_d = 1.9$ (assigned by Du Plessis and Woudberg, 2008.

The reason for the choice of negative powers is because it is expected that c_d should increase with a decrease in average particle shape factor. The value of $\nu = -1$ produces a 25 % increase in c_d at an average particle shape factor of $\phi = 0.8$. Using a value of $\nu = -0.5$ yields an increase of 12 % in c_d at the same average particle shape factor value. The latter more conservative power of dependence is deemed more realistic and will thus be used in this study.

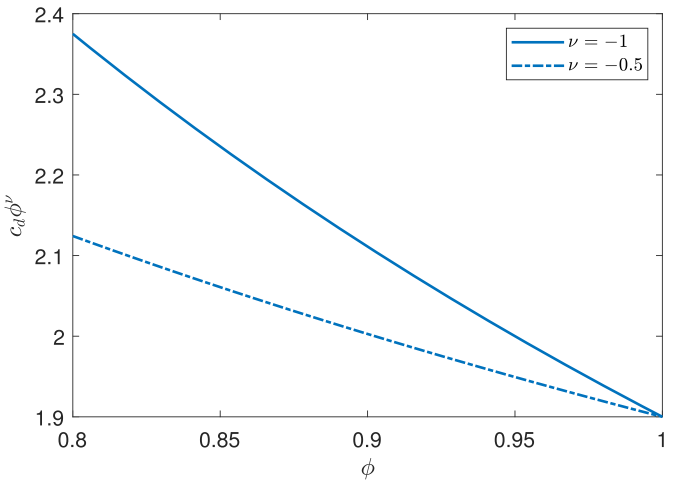

Fig. 2. Power analysis of interstitial form drag coefficient and average particle shape factor product.

2.3. Combined flow regimes

Combining the expressions for the Darcy (Eq. (19)) and Forchheimer (Eq. (21)) flow regimes yield the resulting pressure gradient prediction for the granular RUC model including surface roughness, i.e.

$$\frac{\Delta p}{L} = \frac{25.4\,(1-\epsilon)^{4/3}}{(\phi\, d_s)^2 \left(1-(1-\epsilon)^{1/3}\right)\left(1-(1-\epsilon)^{2/3}\right)^2} \mathcal{R}\,\mu\, q + \frac{c_d\,(1-\epsilon)}{2\left(1-(1-\epsilon)^{2/3}\right)^2 \epsilon\,\phi^{3/2}\, d_s} \mathcal{R}\,\rho\, q^2. \tag{22}$$

Eq. (22) can be used to predict the pressure gradient for rough isotropic granular porous media. It is evident from Eqs. (10), (16) and (19), that setting either k or h_{avg} equal to zero would result in $\delta = 0$ and $\sigma = 0$, yielding $\mathcal{R} = 1$, thus representing smooth particle surfaces.

In order to make Eq. (22) applicable for predicting the pressure drop over a biofilter, the porosity must be adapted by incorporating Eq. (3) to account for biofilm development (i.e. biofilm thickness) and this will be done in Section 4. In the next section the experimental procedure followed for measuring the average surface roughness of the granular packing material used in the experiments of Dumont et al. (2012) will be discussed.

3. Experimental results

Dumont et al. (2012) investigated the performance of expanded schist as packing material for H_2S biofiltration to determine, for instance, its removal efficiency. The expanded schist was chosen due to its homogeneous shape and size distribution, with an average diameter of 10 mm. Three biofilters were studied by Dumont et al. (2016) with expanded schist as packing material and operated for 107 days. As in the study of Woudberg et al. (2019), only the experimental data provided for the first biofilter will be used in this study. On days 0, 19, 39, 57, 71, 92 and 106, the following experimental data were recorded: pressure drop values, volumetric flow rates, from which the superficial velocity values are calculated, as well as the porosity.

A confocal microscope was used to capture the surface topography. Three expanded schist samples were randomly selected, and based on the degree of roughness, labelled as “rough”, “medium” and “smooth”. The “smooth” sample is still rough, but has the least roughness (from what the eye could see) compared to the other two samples.

To ensure accurate height measurements, samples were mounted as flat as possible on an adjustable base plate, reducing z-step variations during data acquisition. A smooth plate served as a reference. Data analysis was performed using µSurf software from Nanofocus to determine the arithmetic absolute average roughness R_a based on three roughness measurements. The samples were gold-coated using a DC sputter coating system to enhance light reflection for improved confocal imaging as shown in Fig. 3.

Fig. 3. Gold coated expanded schist sample (left) versus non-coated sample (right).

Although the lateral resolution is theoretically limited by the light’s wavelength, in this study, it was constrained by the objective lens’ field of view and the CCD camera’s pixel density. The confocal data underwent plane correction to remove background irregularities and compensate for sample tilt, ensuring a more accurate representation of surface features.

The average roughness height value is indicated in Fig. 4 and defined as

$$R_a = \frac{1}{L}\int_0^L |r(x)|\,dx\,, \tag{23}$$

where $r(x)$ denotes the roughness height in the vertical y direction over a displacement in the x direction over a total measuring distance L. The µSurf software makes use of the DIN EN ISO 4287 standard when calculating the finite lateral correlation length. The total measuring distance L is divided into sub-lengths l_R, such that $L = 5\, l_R$. The R_a value differs from the RMS (root mean square) roughness value R_q, which is defined as

$$R_q = \sqrt{\frac{1}{L}\int_0^L (r(x))^2\,dx}. \tag{24}$$

The R_a value is easier to define and measure than R_q and gives a good general description of height variations for roughness elements (Gadelmawla et al., 2002). Furthermore, R_a is not as sensitive to small changes in the roughness profile compared to the R_q. The former, less sensitive parameter R_a is used as the preferred roughness parameter for this study.

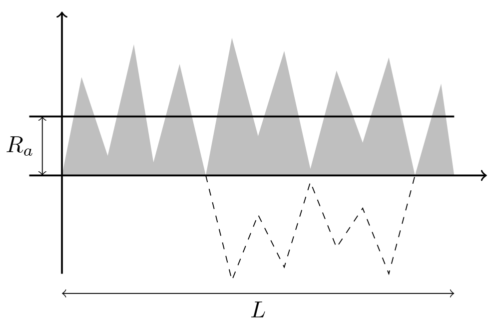

Fig. 4. Average roughness computed with µSurf.

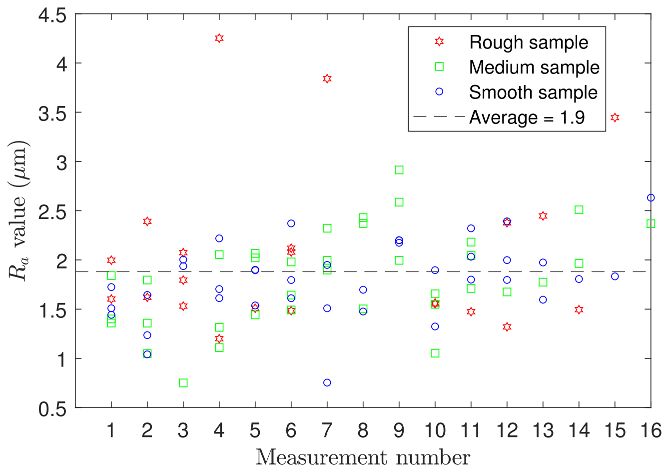

Fig. 5. Confocal height measurements of "rough", "medium" and "smooth" schist samples.

The R_a-values obtained for the three samples are shown in Fig. 5.

The average R_a-value for the "rough" sample is 2.1 μm and 1.8 μm for both the "medium" and "smooth" samples. The R_a-value for the "medium" sample is slightly higher than that of the "smooth" sample when decimal values are included. The roughness values could be measured accurate to four significant figures. The average R_a-value calculated from the three samples is 1.9 μm. This value will thus be used as the h_{avg}-value in the RUC model prediction.

4. Model validation

In this section the pressure gradient prediction of the granular RUC model including surface roughness (given by Eq. (22)) will first be validated against the experimental pressure gradient data obtained from Allen et al. (2013) for airflow through a packed bed of wooden cubes. Thereafter, the model will also be compared to the experimental data obtained from Dumont et al. (2012) as well as to Eqs. (4) and (5), similarly as was done by Woudberg et al. (2019) for the existing granular model taking ϵ_f and ϕ into account.

4.1. Data of Allen et al. (2013)

The wooden cubes investigated by Allen et al. (2013) are uniform, each with an equivalent particle diameter of 16.2 mm and measured surface roughness of 7 μm. The objective was to investigate the effect of particle shape on the pressure drop. They compared their obtained experimental data to an empirical friction factor model for smooth spheres and found the model to under-predict the data by almost 200%. The empirical friction factor f is obtained from their own experimental data for randomly packed smooth spheres (i.e. glass marbles) as well as experimental data obtained by Kays and London (1984), also for smooth spheres, yielding

$$f = \frac{\Delta p}{L}\,\frac{1}{(\rho\, q^2/2)}\,\frac{\epsilon^3}{(1-\epsilon)}\,\frac{4\,\Sigma V_p}{\Sigma A_p} = \frac{172}{Re} + \frac{4.36}{Re^{0.12}}, \tag{25}$$

with the Reynolds number Re defined as

$$Re = 4\,\frac{\rho\, q}{\mu\,(1-\epsilon)}\,\frac{\Sigma V_p}{\Sigma A_p}. \tag{26}$$

In Eqs. (25) and (26), V_p and A_p represent the total volume and surface area of the particles, respectively, and $\Sigma V_p / \Sigma A_p$ represents the pore size, rather than an equivalent particle size.

Allen et al. (2013) expressed the friction factor for the Ergun equation f_{Erg} as

$$f_{Erg} = \frac{\Delta p}{L}\,\frac{1}{(\rho\, q^2/2)}\,\frac{\epsilon^3}{(1-\epsilon)}\,\frac{4\,\Sigma V_p}{\Sigma A_p} = \frac{8}{9}\,\frac{150}{Re} + \frac{4}{3}\,1.75. \tag{27}$$

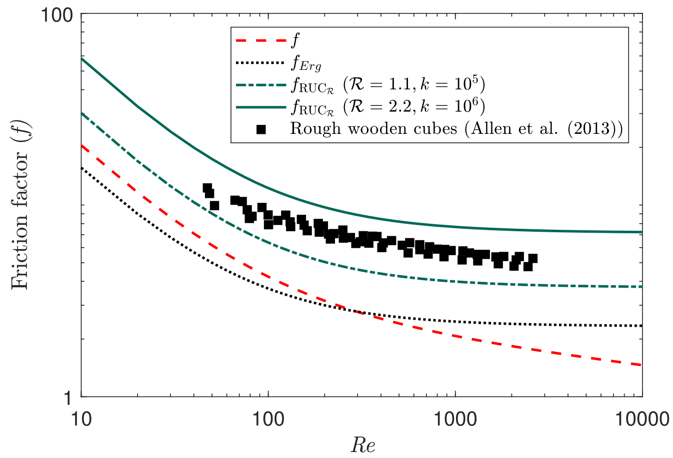

Fig. 6. Log-log plot of the friction factor versus Reynolds number for rough wooden cubes (Allen et al., 2013).

The friction factor for the RUC$_\mathcal{R}$ model $f_{\mathrm{RUC}_\mathcal{R}}$ (given by Eq. (22)) can similarly be expressed as

$$\begin{aligned} f_{\mathrm{RUC}_\mathcal{R}} &= \frac{\Delta p}{L}\,\frac{1}{(\rho\, q^2/2)}\,\frac{\epsilon^3}{(1-\epsilon)}\,\frac{4\,\Sigma V_p}{\Sigma A_p} \\ &= \frac{8}{9}\,\frac{25.4\,(1-\epsilon)^{4/3}\,\epsilon^3\,\mathcal{R}}{\phi^2\left(1-(1-\epsilon)^{1/3}\right)\left(1-(1-\epsilon)^{2/3}\right)^2(1-\epsilon)^2}\,\frac{1}{Re} \\ &\quad + \frac{4}{3}\,\frac{c_d\,\epsilon^2\,\mathcal{R}}{2\,\phi^{3/2}\left(1-(1-\epsilon)^{2/3}\right)^2}, \end{aligned} \tag{28}$$

with $\mathcal{R}$ defined by Eq. (19) and Re defined by Eq. (26).

Fig. 6 shows the experimental data of Allen et al. (2013) for the friction factor f versus Reynolds number Re for rough wooden cubes. Eqs. (25), (27) and (28) are plotted for comparison and it is clear that f (i.e. Eq. (25)) and f_{Erg} (i.e. Eq. (27)) under-predict the data. Allen et al. (2013) report that for $50 < Re < 100$, f under-predicts the data by $85 - 90\,\%$ and for $1900 < Re < 2300$ it under-predicts the data by $180 - 185\,\%$, which is rather significant. Allen et al. (2013) attribute it to the particle shape.

The $f_{\mathrm{RUC}_\mathcal{R}}$ model includes the effects of surface roughness as well as particle shape, i.e. through the average particle shape factor (refer to Eq. (28)). A value of $\phi = 0.81$, used by Allen et al. (2013), was also used in the $f_{\mathrm{RUC}_\mathcal{R}}$ model, since the packed bed consists of particles of uniform shape. The roughness can be calculated by using Eq. (19) and specifying values for k and h_{avg}. The calculated value of $h_{avg} = 7$ μm, given by Allen et al. (2013), was used together with the equivalent particle diameter of $d_s = 16.2$ mm provided. The only unknown parameter in the $f_{\mathrm{RUC}_\mathcal{R}}$ model is the number of roughness elements k. In Fig. 6 the model predictions are shown for both $k = 10^5$ and $k = 10^6$. The number assigned to k should once again be treated as an order of magnitude estimate and should align with Assumption 2.4. The following analysis proves this to be the case for the chosen parameter values:

Consider the volume and surface area of the RUC solid. The total volume of the RUC solid with roughness is $U_s = d_s^3 + 6\,k\,h_{avg}^3$ and the total surface area is $S_s = 6\,d_s^2 + 6\,(4\,k\,h_{avg}^2)$. The values of $h_{avg} = 7 \times 10^{-6}$ m and $d_s = 0.016$ m are fixed and using $k = 10^x$, with $x = 6$ as an arbitrary estimate, a volume of $U_s = d_s^3 + 6\,k\,h_{avg}^3 = 4.1 \times 10^{-6} + 2.1 \times 10^{-9}\ \mathrm{m}^3 \approx d_s^3$ is obtained. The same argument holds for the smaller value of $k = 10^5$. This implies that the added volume due to particle roughness is negligible. The surface area is $S_s = 6\,d_s^2 + 24\,k\,h_{avg}^2 = 1.5 \times 10^{-3} + 1.2 \times 10^{-3}\ \mathrm{m}^2$, and since the contribution of both the particle solid and roughness elements have the same order of magnitude (i.e. 10^{-3}), the surface area of the roughness is not negligible in this case. A value of $k = 10^7$ is excluded since it yields a surface area of $S_s = 6\,d_s^2 + 24\,k\,h_{avg}^2 = 1.5\times10^{-3} + 1.2\times10^{-2}$ m^2, which implies that the surface area of the roughness elements has a higher order of magnitude than that of the solid itself. This would be unrealistic. An order of magnitude lower than 10^5 yields insignificant roughness values for this experiment and are thus also excluded. The upper and lower bounds for k, i.e. 10^6 and 10^5 are substituted into Eq. (19) to determine the corresponding $\mathcal{R}$-values, yielding 2.2 and 1.1, respectively. It is evident from Fig. 6 that the two model predictions satisfactorily enclose the data. It can thus be concluded that the roughness value should lie somewhere in between 1.1 and 2.2 and accounting for the particle shape alone would prove inaccurate. The average relative percentage errors (ARPE's) are given in Table 1 for the different model predictions shown in Fig. 6. The ARPE of the higher and lower $f_{\mathrm{RUC}_\mathcal{R}}$ model predictions are close in magnitude and lower than that of the other model predictions considered. The $f_{\mathrm{RUC}_\mathcal{R}}$ model, originating from Eq. (22), thus shows competence in the prediction capabilities with the inclusion of roughness and the average shape factor.

Table 1
Average relative percentage errors (ARPE's) calculated for friction factor model predictions with respect to experimental data of Allen et al. Allen et al. (2013).

Model	ARPE (%)
f	58
f_{Erg}	57
$f_{\mathrm{RUC}_\mathcal{R}}$ ($\mathcal{R} = 1.1$, $k = 10^5$)	28
$f_{\mathrm{RUC}_\mathcal{R}}$ ($\mathcal{R} = 2.2$, $k = 10^6$)	38

4.2. *Biofiltration data of Dumont et al. (2012)*

Fig. 7 shows the pressure gradient divided by the superficial velocity ($\Delta p/(L\,q)$) for the first day (i.e. day 0) of measurements. On this day there was no biofilm present and hence $L_f = 0$. This, in turn, implies that the biofilm-affected porosity is equal to the initial porosity, i.e. $\epsilon_f = \epsilon_0 = 0.423$. The model predictions presented in Fig. 7 are Eq. (22), labelled as $\mathrm{RUC}_\mathcal{R}$, Eq. (5), labelled as RUC_α, and Eq. (4), representing the modified Ergun equation. Note that the average shape factor is taken to be one ($\phi = 1$) for the $\mathrm{RUC}_\mathcal{R}$ model on day 0, to serve as a reference. It will, however, not be incorrect to say that the average particle shape factor on day 0 being equal to 1 represents that of a sphericity equal to 1, thus assuming the average particle shape on day zero is spherical. It is indeed true, that for a cubic shape, with lower ϕ value, the outer solid surface area is larger than that of a sphere (if the cubic dimension is set equal to the radius of the sphere) and hence the surface roughness also increases, but this is not true for all particle shapes.

For the RUC_α model an initial value of $\phi = 0.85$ on day 0 was chosen for this model to be in consensus with the sphericity calculated by Dumont et al. (2016). From Fig. 7 it can be seen that the slope of the RUC_α model is in good agreement with that of the experimental data, but under-predicts the data. The slope of the modified Ergun equation, however does not follow that of the data and over-predicts at higher superficial velocity values, whilst providing accurate predictions at lower superficial velocity values.

In order to calculate $\mathcal{R}$, estimated values of k need to, once again, be determined. The same procedure of an order-of-magnitude analysis was followed as in the case of the model validation with the data of Allen et al. (2013). In this case, the values of $h_{avg} = 1.9\times10^{-6}$ m and $d_s = 0.01$ m are fixed. For $k = 10^x$, with $x = 7$ the added volume due to particle roughness is, once again, negligible. The surface area of the roughness is again found to be significant. An estimate of $k = 10^8$ results in a surface area of the roughness elements to be of a higher order of magnitude than that of the solid itself, which is unrealistic. An estimate of $k = 10^7$ as order of magnitude is thus used as an upper limit in this case. An

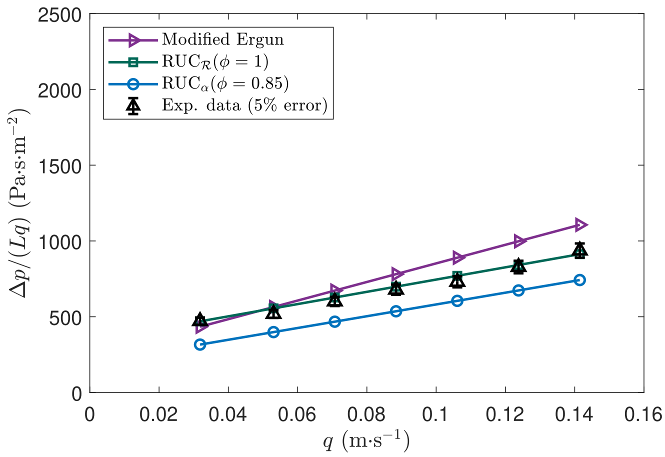

Fig. 7. Pressure gradient prediction divided by superficial velocity versus superficial velocity for day 0.

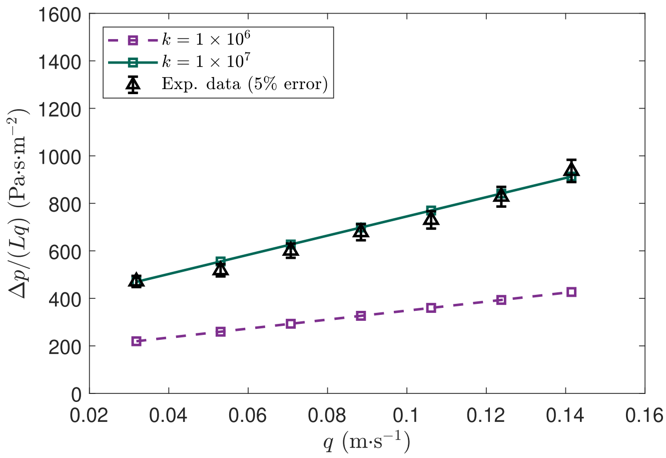

Fig. 8. Sensitivity analysis of k on day 0.

order of magnitude lower than 10^7 yields insignificant roughness values for this experiment and are thus also excluded. Fig. 8 shows the pressure gradient divided by the superficial velocity on day 0 for values of $k = 10^6$ and $k = 10^7$.

An order of magnitude estimate of $k = 10^6$, yields a $\mathcal{R}$-value in the order of unity and hence does not yield a sufficient increase in surface roughness to provide accurate predictions on day 0. The significantly lower pressure gradient divided by the superficial velocity predictions is also evident in Fig. 8. It can be concluded that the order of magnitude for the number of roughness elements has a significant effect on the roughness and hence also the pressure gradient divided by the superficial velocity predictions. The estimate of $k = 10^7$ thus proved to be adequate, and just to, once again emphasize, is merely an order of magnitude estimate, rather than an exact value. The value of 10^7 for k has been used in Eq. (19) to determine the value of $\mathcal{R}$, which is used in the $\mathrm{RUC}_\mathcal{R}$ model prediction for all the days of biofilter operation. The pressure gradient prediction provided by the $\mathrm{RUC}_\mathcal{R}$ model is also shown in Fig. 7. An average relative percentage error of 3 % is obtained with respect to the experimental data.

Figs. 9–11 show the pressure gradient divided by the superficial velocity versus the superficial velocity for the remaining days of the experiment (i.e. days 19, 39, 57, 71, 92 and 106). The $\mathrm{RUC}_\mathcal{R}$, RUC_α and modified Ergun model predictions are again compared to the experimental data. On these days biofilm was present and allowed to develop freely. The porosity values on each day of biofilter operation is given in Table 2. These values were determined experimentally by Dumont

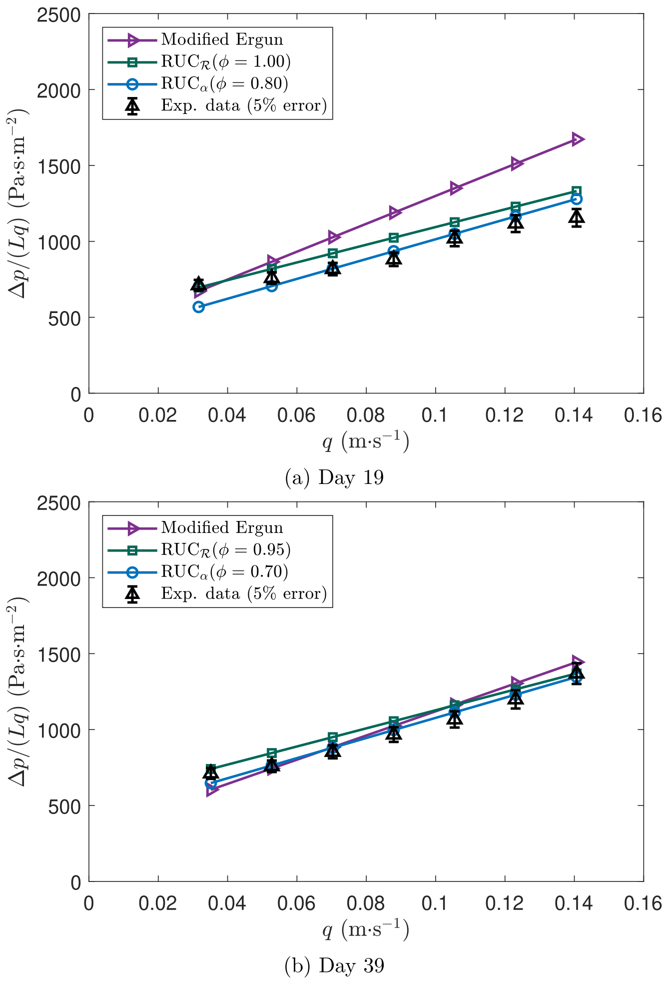

Fig. 9. Pressure gradient divided by superficial velocity versus superficial velocity for (a) day 19 and (b) day 39.

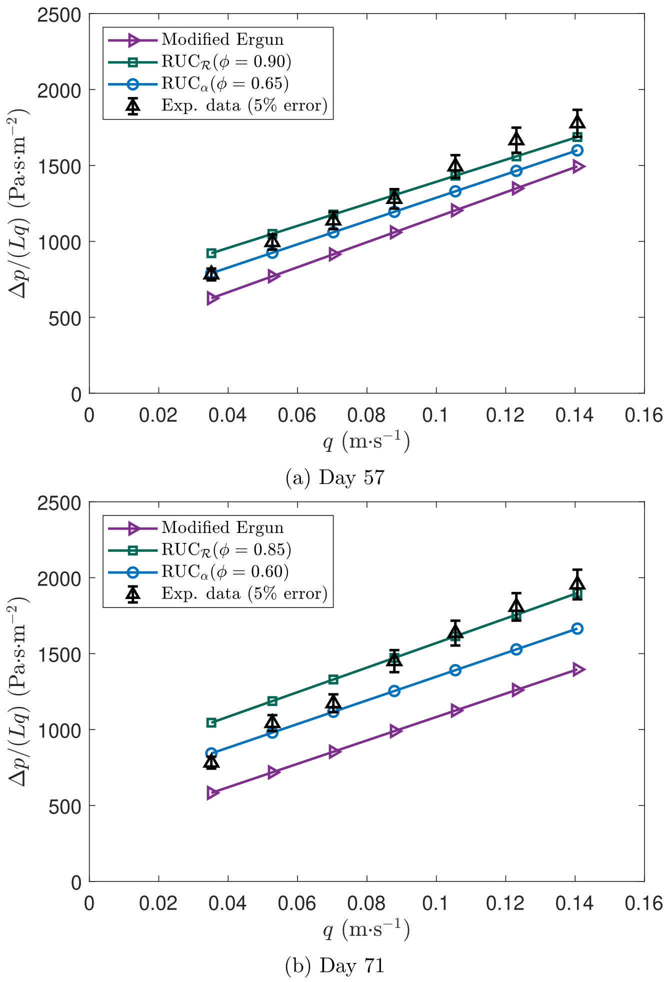

Fig. 10. Pressure gradient divided by superficial velocity versus superficial velocity for (a) day 57 and (b) day 71.

et al. (2012). The biofilm-affected porosity values (i.e. ϵ_f-values given in Table 2) were determined theoretically by using Eq. (3), together with a coordination number of $n = 7$ (Woudberg et al., 2019), the initial porosity $\epsilon_0 = 0.4230$, a particle radius of $R = 5\,\mathrm{mm}$ and the biofilm thickness values L_f (also given in Table 2 for the respective days). The coordination number and biofilm thickness values were determined by Dumont et al. (2016) and used by Woudberg et al. (2019) in their previous study. The latter values are also used in this study for the model predictions. Hence the calculated ϵ_f-values are used in the modified Ergun, RUC_α and $\mathrm{RUC}_\mathcal{R}$ equations for the pressure drop predictions. Note furthermore that an increase in $\mathcal{R}$ does not imply that the particles are getting rougher over time (i.e. biofilter operation) since a constant value is used for h_{avg} in Eq. (19), but rather that the effect of surface roughness is increasing. This is consistent with the findings of Dumont et al. (2016) and Woudberg et al. (2019).

Recall the $\mathrm{RUC}_\mathcal{R}$ and RUC_α models have been adapted to account for surface roughness as well as sphericity (or rather average particle shape), whilst the modified Ergun equation only accounts for surface roughness. Recall, furthermore, the RUC_α and modified Ergun equations have fixed roughness values, whilst the $\mathrm{RUC}_\mathcal{R}$ model includes the variable roughness factor. In the present study, both parameters are allowed to vary.

In Figs. 7–11 it is evident with regards to the experimental data points, that not only is there a clear increase in each pressure gradient divided by superficial velocity value over time for the same superficial velocity for the different consecutive days, but the overall slope of the data increases as well. This increase implies that the flow experiences more resistance over time due to biofilm development. Woudberg et al. (2019) concluded that the increase in the slope of the data is due to a decrease in sphericity caused by the biofilm development and surface roughness not accounted for. This was justified by the fact that the modified Ergun equation with constant roughness and sphericity of $\phi = 1$, fails to predict the change in data over time. This modified Ergun equation over-predicts the experimental data on day 19, corresponds well on day 39 and then under-predicts on days 57 to 106. The slope of the modified Ergun equation, however, corresponds well to that of the data.

Figs. 7–11 show that on day 19 the RUC_α model under-predicts and over-predicts the data for low and high superficial velocity values, respectively, corresponds well to the data on day 39, and under-predicts the data further on, with an exception on day 92. On day 0 the model

Table 2
Summary of important parameters.

Days	ϵ	ϵ_f	L_f (m)	ϕ	$\mathcal{R}$	ARPE's (%)
0	0.423	0.423	0	1.00	2.45	3
19	0.388	0.385	1.12×10^{-4}	1.00	2.45	10
39	0.405	0.397	7.30×10^{-5}	0.95	2.61	7
57	0.409	0.392	8.20×10^{-5}	0.90	2.79	2
71	0.411	0.397	6.40×10^{-5}	0.85	3.01	8
92	0.392	0.377	1.22×10^{-4}	0.90	2.79	13
106	0.398	0.371	1.39×10^{-4}	0.90	2.79	-4

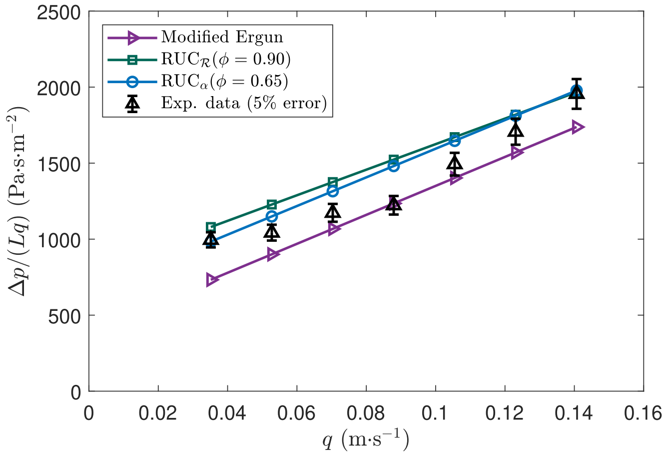

(a) Day 92

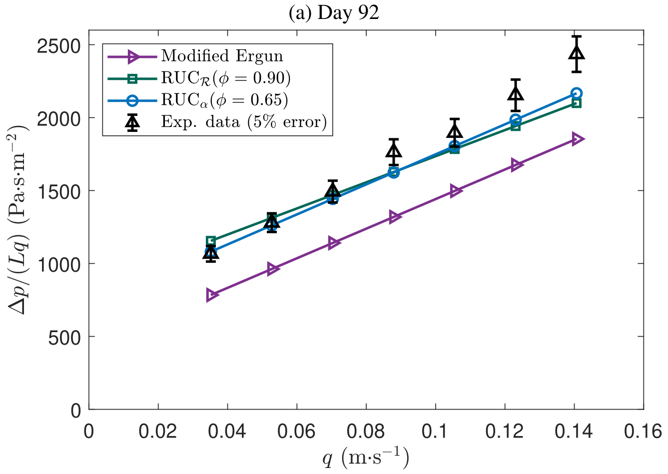

(b) Day 106

Fig. 11. Pressure gradient divided by superficial velocity versus superficial velocity for (a) day 92 and (b) day 106.

commences with a sphericity of $\phi = 0.85$. Note that no biofilm was yet present on this day. This value drops to $\phi = 0.80$ on day 19, $\phi = 0.70$ on day 39 and then $\phi = 0.65$ for the remaining days, with an exception on day 71, where it had a value of $\phi = 0.60$. The sphericity values for the RUC_α model presented here are ones chosen by Woudberg et al. (2019) to yield the best fit to the experimental data. The variable sphericity could be justified by the dynamic development of biofilm around more than one particle thus forming clusters of particles that deviate from the spherical shape. These ϕ-values are rather low in comparison to the value of $\phi = 0.85$ calculated by Dumont et al. (2016). The RUC_α model accounting for variable sphericity and constant roughness, however, proves to be more accurate than the modified Ergun equation, and has an average absolute relative percentage error of 7.6 %. The latter value has been calculated by adding the average relative percentage difference values obtained for each day and then calculating the average absolute value.

Figs. 7–11 show that the $\mathrm{RUC}_{\mathcal{R}}$ model provides the most accurate predictions amongst the three models considered. A summary of the average relative percentage errors (ARPE's) is given in Table 2. The average absolute relative percentage error for this model is 6.6 %. Also given in Table 2 are the average shape factor values used in the $\mathrm{RUC}_{\mathcal{R}}$ model. These values are closer to the value of 0.85 computed by Dumont et al. (2016), than that of the RUC_α model. Since ϕ represents an average value in the $\mathrm{RUC}_{\mathcal{R}}$ model, these values also seems more realistic than those used in the RUC_α model. Since a constant roughness value was used in the RUC_α model, it may be that the increase in pressure gradient over time was over-compensated by the sphericity in the latter

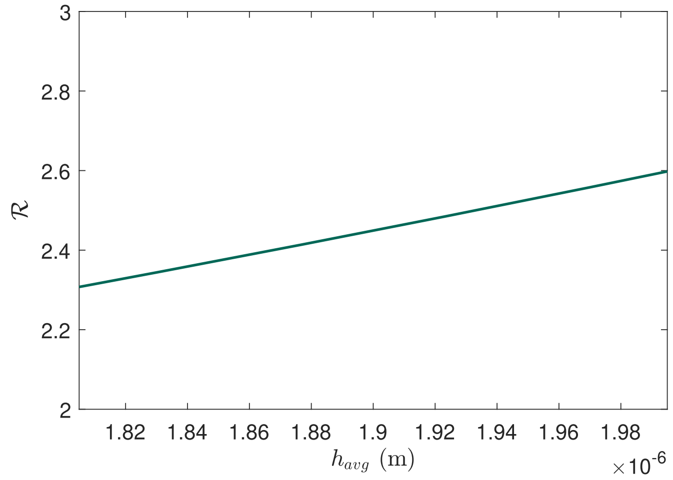

Fig. 12. Roughness $\mathcal{R}$ versus average height of roughness elements h_{avg}.

model. From Figs. 9–11 it can be seen that the slope of the $\mathrm{RUC}_{\mathcal{R}}$ model corresponds slightly less to that of the experimental data than that of the modified Ergun equation. The ARPE's for all the days, however, are satisfactory with the lowest values being on days 0, 57 and 106. It seems that a variable roughness and average shape factor provides the most accurate results.

Table 2 furthermore shows that the roughness factor varies between about 2.5 and 3.0, which is significant and hence need to be accounted for, although the biofilm thickness varies within the order of 10^{-4} and 10^{-5} and does not have a significant effect on the porosity.

In the next section a sensitivity analysis will be done on the $\mathrm{RUC}_{\mathcal{R}}$ model on day 0 to investigate the effect of small changes in some model input parameters on the model predictions.

5. Sensitivity analysis

In this section a sensitivity analysis will be done on the parameters that influence the surface roughness $\mathcal{R}$, namely, h_{avg}, ϕ, d_s and ϵ (refer to Eq. (19)). A discussion on the justification for the choice of ϕ will also be done. (It has already been done in Section 4 for k.)

Recall that the measured value for h_{avg} is 1.9×10^{-6} m. Fig. 12 shows the roughness $\mathcal{R}$ versus the average height of roughness elements h_{avg}. The expected increase in roughness with average roughness height is observed. An increase of 5 % in h_{avg} (i.e. from 1.9×10^{-6} m to 2.0×10^{-6} m), yields a 6 % increase in $\mathcal{R}$. Furthermore, a decrease of 5 % in h_{avg} (i.e. from 1.9×10^{-6} m to 1.8×10^{-6} m) yields a decrease of 5.8 % in $\mathcal{R}$. The change in $\mathcal{R}$ is thus moderate (if larger than 10 % is regarded as high and below 5 % as low) for an error of ± 5 % in h_{avg}.

Fig. 13 shows the effect of small changes in $\mathcal{R}$ on the proposed pressure gradient model $\mathrm{RUC}_{\mathcal{R}}$ as a result of an ± 5 % error in h_{avg}. The data is plotted with 5 % uncertainty. The average increase of the model predictions in $\Delta p/(Lq)$ due to the increase in h_{avg} is 6.1 % and the average decrease due to the decrease in h_{avg} is 5.8 %. It can be concluded that the model predictions are also moderately sensitive for an error of ± 5 % in h_{avg}.

Fig. 14 shows the roughness factor $\mathcal{R}$ plotted against the particle diameter d_s, where d_s ranges within ± 5 % (i.e. from 9.5 mm to 10.5 mm). Recall that the average diameter for the expanded schist used was 10 mm. Fig. 14 illustrates that a 5 % decrease in the particle diameter yields a 6.4 % increase in the surface roughness and a 5 % increase in the particle diameter yields a 5.6 % decrease in the roughness value. These results make sense from a physical point of view since smaller objects have larger surface areas per unit volume.

Fig. 15 shows the effect that a change of ± 5 % in the particle diameter d_s has on the pressure gradient model $\mathrm{RUC}_{\mathcal{R}}$. Note that a change in d_s not only changes the pressure gradient through the surface roughness,

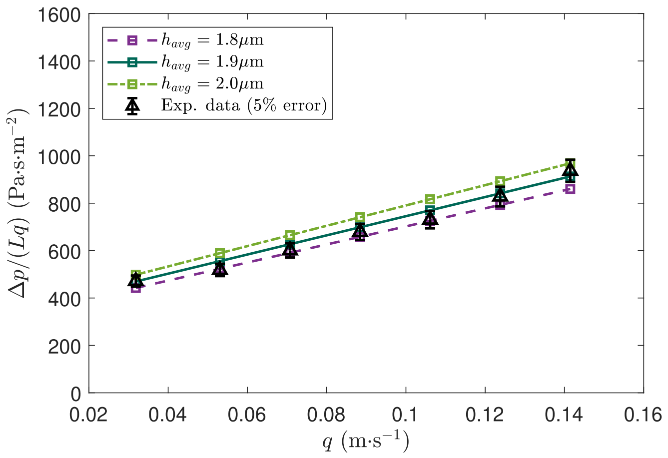

Fig. 13. Sensitivity analysis of h_{avg} on $\Delta p/(Lq)$ for day 0.

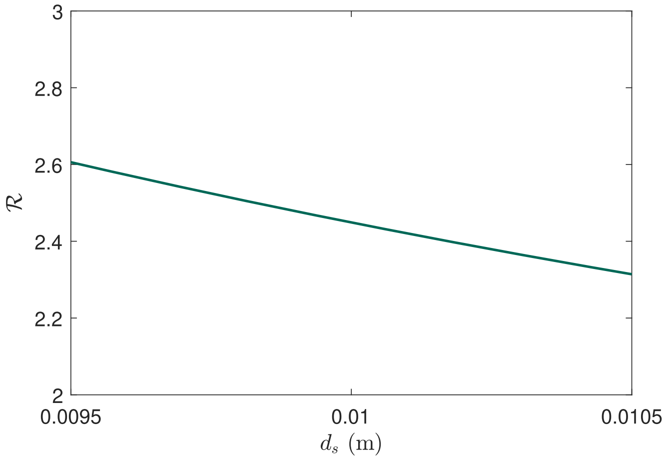

Fig. 14. Roughness $\mathcal{R}$ versus the particle diameter d_s.

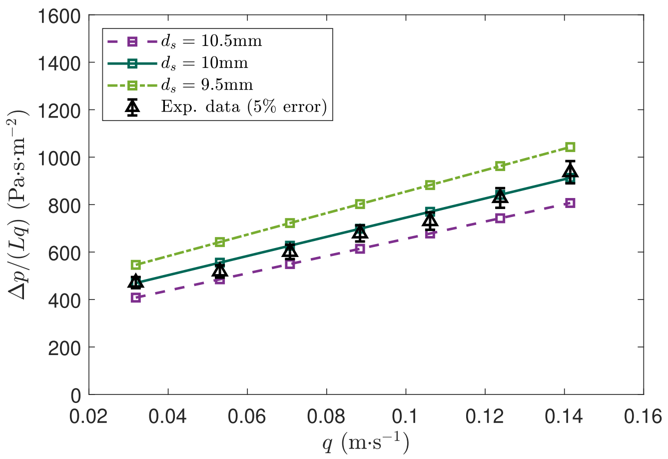

Fig. 15. Sensitivity analysis of d_s on $\Delta p/(Lq)$ for day 0.

but also directly through its incorporation in Eq. (22). It is found that an increase of 5 % in the particle diameter yields an average decrease of 12.1 % in $\Delta p/(Lq)$. Furthermore, a 5 % decrease in d_s yields an average increase of 14.9 % in the pressure gradient. Thus, it can be concluded that the model predictions are highly sensitive to changes of ±5 % in the measured average d_s value used.

For a sensitivity analysis on the average particle shape factor, only a decrease in percentage is considered, since $\phi = 1$ is used for day 1, which is the maximum value that this parameter can take on. Fig. 16

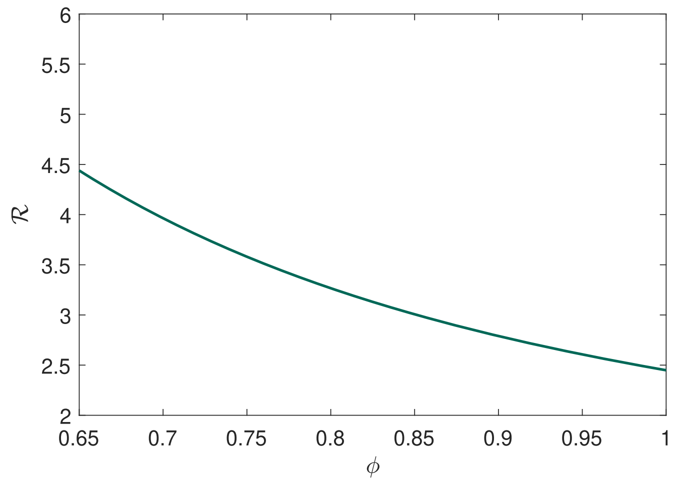

Fig. 16. Roughness $\mathcal{R}$ versus average particle shape factor ϕ.

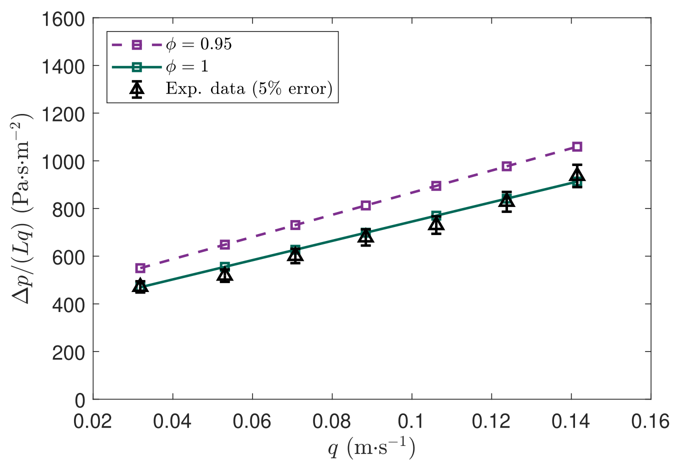

Fig. 17. Sensitivity analysis of ϕ on $\Delta p/(Lq)$ for day 0.

shows the decrease in roughness as the average particle shape factor increases and should be interpreted as how a change in the average shape factor influences the roughness factor. This change in average particle shape factor is also implicitly due to biofilm attaching and detaching as well as developing over clusters of particles during biofilter operation, thus changing the overall average shape of the packing material. How and to what degree these changes take place is extremely complicated to determine, also from an experimental point of view. Table 2 shows that the biofilm thickness increased and then decreased, followed by another increase over time. The average shape factor also decreased and increased over time, since these effects are interrelated. This, in turn, also led to an increase and decrease in the roughness factor, following the dependence portrayed by Fig. 16. Note that the measured average roughness height of the schist remained constant over the different days of biofilter operation, although the roughness “effect” changed, because this parameter is dependent not only on the average particle shape factor and average roughness height, but also on the average particle diameter, porosity and number of roughness elements, which are all interrelated. The introduction of the average shape factor should thus be regarded as a first-order approach in understanding the complex physical phenomena taking place with an operating biofilter. We can at most say from the present analysis, that the roughness effect increases with a decrease in average particle shape. Further experimental studies combined with in-depth mathematical modelling analyses are required to investigate and refine the physical dependencies of the different parameters involved. A 5 % decrease in the average particle shape factor (i.e. from $\phi = 1$ to $\phi = 0.95$) yields an increase of 6.4 % in the surface roughness factor $\mathcal{R}$.

Fig. 17 shows the effect of a 5 % decrease in the average particle shape factor ϕ on the pressure gradient predicted by the RUC$_{\mathcal{R}}$ model. Note that ϕ influences Eq. (22) directly as well as through the surface roughness $\mathcal{R}$. It is found that a decrease of 5 % in the average particle shape factor yields an average increase of 16.4 % in the pressure gradient ratio. It can be concluded that the model predictions are highly sensitive to a decrease of 5 % in the average ϕ value used.

The change in roughness factor for a ± 5 % change in ϵ, is not shown graphically, because the effect on $\mathcal{R}$ is negligible.

6. Conclusions

The proposed RUC$_{\mathcal{R}}$ model which accounts for the effect of particle roughness is an improvement on the existing RUC$_{\alpha}$ model, which excludes roughness and can predict the pressure gradient of the biofilter considered with reasonable accuracy (i.e. < 10 % error). It was found that varying the roughness factor as well as the average particle shape factor over time is a preferable approach compared to the previous approaches in which these parameters have been assumed constant. The average roughness height of the expanded schist, used as packing material in the biofilter, has been measured successfully. As opposed to the former models, the average particle shape factor has been introduced in the Forchheimer term through both the average particle diameter and the interstitial form drag coefficient. An analytical expression is derived for the particle surface roughness factor which is introduced into both the Darcy and Forchheimer terms of the proposed model. The roughness factor amounts to values of between 2 and 3, which is not negligible. The need to take particle roughness into account is highlighted by this study through a graphical comparison with two sets of pressure gradient data and the under-prediction of existing models which excludes particle roughness. It was found that the roughness factor is moderately sensitive (i.e. between 5 and 10 %) to the average roughness height and average particle diameter, highly sensitive to the average particle shape factor and is not affected by the porosity. The pressure gradient is moderately sensitive (i.e. between 5 and 10 %) to the average roughness height and highly sensitive to both the average particle diameter and sphericity. The advantages of the novel proposed RUC$_{\mathcal{R}}$ model are, first of all, its physical adaptive capabilities to extend its range of applicability. This has been illustrated in the present study through the originality of adding cubic surface roughness elements to the granular RUC model, together with the introduction of a roughness factor. The latter parameter is derived from physical principles and expressed in terms of physical geometric parameters. The model is user friendly, in the sense that the geometric input parameters are measurable quantities (e.g., porosity, average particle diameter and average height of roughness elements), whilst range estimates can be determined for the total number of roughness elements and the change in the average particle shape factor. These properties, together with their relative geometric and mathematical simplicity, render the model favourable in comparison to the fractal models for which the fractal parameters are often significantly more complicated to assign values to in compliance with the physical measurable parameters. Since the proposed RUC$_{\mathcal{R}}$ model is, in addition, not fluid or packing material specific, it is applicable to biofilters in general. Further model validation with other data sets is, however, recommended as well as future studies to refine the interdependent effect of the biofilm thickness and development on the average particle shape factor and roughness factor. The findings of this study have the potential to aid in the improvement of optimization in biofiltration systems, and contribute to a deeper understanding of surface roughness characterization.

CRediT authorship contribution statement

R. J. Van Velden: Conceptualization, Writing – original draft, Validation, Investigation, Visualization, Methodology, Formal analysis; **S. Woudberg:** Writing – review & editing, Project administration, Resources, Formal analysis, Supervision, Validation, Conceptualization, Methodology, Investigation; **E. Dumont:** Resources, Validation, Investigation, Writing – review & editing, Data curation; **H. Fidder:** Validation, Data curation, Writing – review & editing, Investigation, Resources; **J.Th.M. De Hosson:** Writing – review & editing, Resources, Formal analysis, Conceptualization, Validation, Data curation, Methodology, Investigation.

Data availability

Data will be made available on request.

Declaration of competing interest

The authors declare that they have no known competing financial interests or personal relationships that could have appeared to influence the work reported in this paper.

Acknowledgment

The first author is truly grateful for financial support from the Wilhelm Frank scholarship, which assisted in the ability to conduct the research. Opinions expressed and conclusions arrived at, are furthermore those of the authors and are not necessarily to be attributed to the scholarship.

Appendix A. Derivation of existing RUC model prediction

The following derivation is a summary of the model of Du Plessis and Woudberg (2008). All the equations presented in this section come from the work of Du Plessis and Woudberg (2008). These authors have applied volume averaging (Bachmat and Bear, 1986) to the continuity and Navier-Stokes equations and assumed a uniform superficial velocity, yielding the following expression for the streamwise pressure gradient for the Darcy flow regime

$$\frac{\Delta p}{d} = \frac{S_{||}\,\tau_{w_{||}} + \xi\, S_{\perp}\tau_{w_{\perp}}}{U_f}\,\psi\,, \tag{A.1}$$

where $S_{||}$ and $S_{\perp}$ denote the total surface area parallel and perpendicular to the streamwise direction, respectively, also referred to as the streamwise and transverse surfaces, respectively, $\tau_{w_{||}}$ and $\tau_{w_{\perp}}$, denote the total average streamwise and transverse wall shear stress, respectively, and U_f is the total fluid volume within the RUC. Furthermore, let $d = L$ for the pressure gradient in Eq. (A.1). The geometric coefficient ξ represents the reduction in tortuosity as a result of the splitting of the streamtube in the transverse channels of a staggered array. The geometric factor ψ is defined as the ratio of the total fluid volume to the total streamwise fluid volume, which can in turn be expressed in terms of the streamwise cross-sectional flow area $A_{p_{||}}$ and simplified to give

$$\psi = \frac{U_f}{A_{p_{||}}\,d}. \tag{A.2}$$

The pore-scale linear dimensions d and d_s are shown in Fig. A.18. The porosity ϵ is defined as the ratio of the total fluid volume U_f over the total volume of the RUC U_o, i.e. $\epsilon = U_f/U_o$. It hence follows that

$$d_s = d\,(1-\epsilon)^{1/3}. \tag{A.3}$$

The geometric factor can consequently be expressed in terms of the RUC dimensions, as follows:

$$\psi = \frac{d^3 - d_s^3}{(d^2 - d_s^2)\,d}. \tag{A.4}$$

The relationship between the transverse average pore velocity $w_{\perp}$ and the streamwise average pore velocity $w_{||}$ is defined as the coefficient

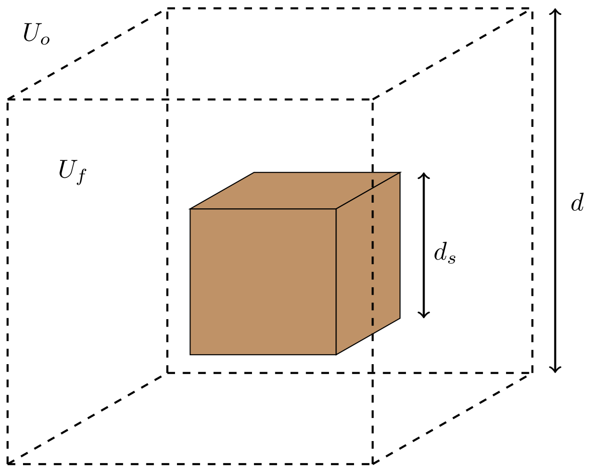

Fig. A.18. Existing granular RUC model.

β. For flow between parallel plates a uniform distance $d - d_s$ apart, it follows that

$$\tau_{w_{||}} = \frac{6\,\mu\,w_{||}}{d - d_s}, \tag{A.5}$$

and hence $\tau_{w_\perp} = \beta\,\tau_{w_{||}}$, such that

$$\frac{\Delta p}{L} = \frac{S_{||} + \beta\,\xi\,S_\perp}{U_f}\,\tau_{w_{||}}\,\psi\ . \tag{A.6}$$

Furthermore, since $w_{||} = q\,\psi/\epsilon$ and $U_f = d^3\,\epsilon$, it follows that

$$\frac{\Delta p}{L} = \frac{6(S_{||} + \beta\,\xi\,S_\perp)}{(d - d_s)\,d^3}\,\frac{\psi^2}{\epsilon^2}\,\mu\,q. \tag{A.7}$$

Note that $S_{||} = 4\,d_s^2$, $S_\perp = 2\,d_s^2$ and $\psi = \epsilon/(1-(1-\epsilon)^{2/3})$. Since for the granular RUC model $\beta = \sqrt{2}$ and $\xi = 1/4$ (Du Plessis and Woudberg, 2008), it follows that

$$\frac{\Delta p}{L} = \frac{25.4\,(1-\epsilon)^{4/3}}{d_s^2\left(1-(1-\epsilon)^{1/3}\right)\left(1-(1-\epsilon)^{2/3}\right)^2}\,\mu\,q. \tag{A.8}$$

For the inertial flow regime, the streamwise pressure gradient is expressed as

$$\frac{\Delta p}{L} = \frac{S_{face}\,\psi^2}{2\,\epsilon^3\,U_o}\,c_d\,\rho\,q^2\ , \tag{A.9}$$

which results from the assumption of interstitial flow recirculation on the lee side of a solid cube. The interstitial form drag coefficient c_d is inferred from the form drag condition for flow past a single obstacle in an infinite stream. The total cross-sectional flow area “facing” upstream is $S_{face} = d_s^2$. Hence, the streamwise pressure gradient can be expressed as

$$\frac{\Delta p}{L} = \frac{(1-\epsilon)}{2\left(1-(1-\epsilon)^{2/3}\right)^2\,\epsilon\,d_s}\,c_d\,\rho\,q^2, \tag{A.10}$$

with $c_d = 1.9$ (Du Plessis and Woudberg, 2008). A superposition of Eqs. (A.8) and (A.10), yields

$$\frac{\Delta p}{L} = \frac{25.4\,(1-\epsilon)^{4/3}}{d_s^2\left(1-(1-\epsilon)^{1/3}\right)\left(1-(1-\epsilon)^{2/3}\right)^2}\,\mu\,q + \frac{(1-\epsilon)}{2\left(1-(1-\epsilon)^{2/3}\right)^2\,\epsilon\,d_s}\,c_d\,\rho\,q^2. \tag{A.11}$$

References

Allen, K.G., Von Backström, T.W., Kröger, D.G., 2013. Packed bed pressure drop dependence on particle shape, size distribution, packing arrangement and roughness. Powder Technol. 246, 590–600. https://doi.org/10.1016/j.powtec.2013.06.022

Alonso, C., Suidan, M.T., Sorial, G.A., Smith, F.L., Biswas, P., Smith, P.J., Brenner, R.C., 1997. Gas treatment in trickle-bed biofilters: biomass, how much is enough? Biotechnol. Bioeng. 54 (6), 583–594. https://doi.org/10.1002/(SICI)1097-0290(19970620)54:6<583::AID-BIT9>3.0.CO;2-F

Bachmat, Y., Bear, J., 1986. Macroscopic modelling of transport phenomena in porous media. 1: the continuum approach. Transp. Porous Media 1, 213–240. https://doi.org/10.1007/BF00238181

Chen, Y., Xie, L., Cai, W., Wu, J., 2019. Pilot-scale study using biotrickling filter to remove H_2S from sewage lift station: experiment and CFD simulation. Biochem. Eng. J. 144, 177–184. https://doi.org/10.1016/j.bej.2019.02.003

Comiti, J., Renaud, M., 1989. A new model for determining mean structure parameters of fixed beds from pressure drop measurements: application to beds packed with parallelepipedal particles. Chem. Eng. Sci. 44 (7), 1539–1545. https://doi.org/10.1016/0009-2509(89)80031-4

Devinny, J.S., Deshusses, M.A., Webster, T.S., 2017. Biofiltration for Air Pollution Control. CRC press.

Du Plessis, J.P., 1994. Analytical quantification of coefficients in the ergun equation for fluid friction in a packed bed. Transp. Porous Media 16, 189–207. https://doi.org/10.1007/BF00617551

Du Plessis, J.P., Masliyah, J.H., 1991. Flow through isotropic granular porous media. Transp. Porous Media 6, 207–221. https://doi.org/10.1007/BF00208950

Du Plessis, J.P., Woudberg, S., 2008. Pore-scale derivation of the ergun equation to enhance its adaptability and generalization. Chem. Eng. Sci. 63 (9), 2576–2586. https://doi.org/10.1016/j.ces.2008.02.017

Dumont, E., 2017. Validation of a rapid procedure to determine biofilter performances. J. Environ. Chem. Eng. 5 (3), 2668–2680. https://doi.org/10.1016/j.jece.2017.05.022

Dumont, E., Ayala Guzman, L.M., Rodríguez Susa, M.S., Andres, Y., 2012. H_2S biofiltration using expanded schist as packing material: performance evaluation and packed-bed tortuosity assessment. J. Chem. Technol. Biotechnol. 87 (6), 725–731. https://doi.org/10.1002/jctb.3713

Dumont, E., Woudberg, S., Van Jaarsveld, J., 2016. Assessment of porosity and biofilm thickness in packed beds using porous media models. Powder Technol. 303, 76–89. https://doi.org/10.1016/j.powtec.2016.08.060

Gadelmawla, E.S., Koura, M.M., Maksoud, T. M.A., Elewa, I.M., Soliman, H.H., 2002. Roughness parameters. J. Mater. Process. Technol. 123 (1), 133–145. https://doi.org/10.1016/S0924-0136(02)00060-2

Hu, Y., Wang, Q., Zhao, J., Xie, S., Jiang, H., 2020. A novel porous media permeability model based on fractal theory and ideal particle pore-space geometry assumption. Energies 13 (3), 510. https://doi.org/10.3390/en13030510

Huang, T., Du, P., Peng, X., Wang, P., Zou, G., 2020. Pressure drop and fractal non-darcy coefficient model for fluid flow through porous media. J. Pet. Sci. Eng. 184, 106579. https://doi.org/10.1016/j.petrol.2019.106579

Kays, W.M., London, A.L., 1984. Compact Heat Exchangers. McGraw-Hill, New York, NY.

Morgan-Sagastume, F., Sleep, B.E., Allen, D.G., 2001. Effects of biomass growth on gas pressure drop in biofilters. J. Environ. Eng. 127 (5), 388–396. https://doi.org/10.1061/(ASCE)0733-9372(2001)127:5(388)

Palasantzas, G., De Hosson, J. T.M., 2000. Roughness effect on the measurement of interface stress. Acta Mater. 48 (14), 3641–3645. https://doi.org/10.1016/S1359-6454(00)00170-1

Prokop, W.H., Bohn, H.L., 1985. Soil bed system for control of rendering plant odors. J. Air Pollut. Control Assoc. 35 (12), 1332–1338. https://doi.org/10.1080/00022470.1985.10466036

Soreanu, G., Dumont, É., 2020. From Biofiltration to Promising Options in Gaseous Fluxes Biotreatment: Recent Developments, New Trends, Advances, and Opportunities. Elsevier.

Tu, B., Xiao, B., Zhang, Y., Long, G., 2024. An analytical model for permeability of fractal tree-like branched networks composed of converging–diverging capillaries. Phys. Fluids 36 (4). https://doi.org/10.1063/5.0201040

Van Loosdrecht, M., Eikelboom, D., Gjaltema, A., Mulder, A., Tijhuis, L., Heijnen, J.J., 1995. Biofilm structures. Water Sci. Technol. 32 (8), 35–43. https://doi.org/10.1016/0273-1223(96)00005-4

Woudberg, S., Van Jaarsveld, J., Dumont, E., 2019. Predicting the pressure drop of a biofilter and the specific surface area of the packing material. Powder Technol. 342, 233–245. https://doi.org/10.1016/j.powtec.2018.09.059

Wu, J., Yu, B.M., 2007. A fractal resistance model for flow through porous media. Int. J. Heat Mass Transf. 50 (19), 3925–3932. https://doi.org/10.1016/j.ijheatmasstransfer.2007.02.009

Xiao, B., Huang, Q., Chen, H., Chen, X., Long, G., 2021. A fractal model for capillary flow through a single tortuous capillary with roughened surfaces in fibrous porous media. Fractals 29 (01), 2150017. https://doi.org/10.1142/S0218348X21500171

Xiao, B., Zhu, H., Chen, F., Long, G., Li, Y., 2023. A fractal analytical model for Kozeny-Carman constant and permeability of roughened porous media composed of particles and converging-diverging capillaries. Powder Technol. 420, 118256. https://doi.org/10.1016/j.powtec.2023.118256

Xu, P., Li, Z., Wang, J., Chen, Q., Qiu, S., 2024. A new fractal pore-throat chain model for non-darcy flow through porous media. Adv. Water Resour. 192, 104782. https://doi.org/10.1016/j.advwatres.2024.104782

Xu, P., Yu, B.M., 2008. Developing a new form of permeability and Kozeny-Carman constant for homogeneous porous media by means of fractal geometry. Adv. Water Resour. 31 (1), 74–81. https://doi.org/10.1016/j.advwatres.2007.06.003

Yang, S., Laing, M.-C., Yu, B.-M., Zou, M.Q., 2015. Permeability model for fractal porous media with rough surfaces. Microfluid. Nanofluid. 18 (19), 1085–1093. https://doi.org/10.1007/s10404-014-1500-1

Yang, S., Yu, B.-M., Zou, M.-Q., Liang, M.C., 2014. A fractal analysis of laminar flow resistance in roughened microchannels. Int. J. Heat Mass Transf. 77, 208–217. https://doi.org/10.1016/j.ijheatmasstransfer.2014.05.016

Yang, Y., Allen, E.R., 1994. Biofiltration control of hydrogen sulfide 1. design and operational parameters. J. Air Waste Manag. Assoc. 44 (7), 863–868. https://doi.org/10.1080/1073161X.1994.10467287

Yu, B.-M., Cheng, P., 2002. A fractal permeability model for bi-dispersed porous media. Int. J. Heat Mass Transf. 45 (14), 2983–2993. https://doi.org/10.1016/S0017-9310(02)00014-5